Journal of Materials Chemistry A

RSC Publishing

PAPER

View Article Online
View Journal

Effects of Al-doping on the properties of Li–Mn–Ni–O cathode materials for Li-ion batteries: an *ab initio* study

Cite this: DOI: 10.1039/c3ta11598d

Arezoo Dianat,[a] Nicola Seriani,[b] Manfred Bobeth*[a] and Gianaurelio Cuniberti[acd]

The key properties of a successful cathode material, such as the structural stability during delithiation, the battery voltage, and the Li mobility, were investigated for Al-doped Li–Mn–Ni oxide structures, using density-functional theory and the nudged-elastic band method. The rhombohedral layered structure of $LiMn_{0.5}Ni_{0.5}O_2$ with zigzag and flower arrangements of transition metal atoms as well as the monoclinic structure of $Li(Li_{1/6}Ni_{1/6}Mn_{2/3})O_2$ were used as base structures. A stabilizing effect of Al-doping was found for all partially lithiated systems considered. The derived battery voltages at zero temperature are generally enhanced by Al-doping. The calculated activation energies for Li jumps suggest slower Li mobility. The Al-doped Li-rich monoclinic structure seems to be most promising as a cathode material because of a comparatively high battery voltage.

Received 22nd April 2013
Accepted 5th June 2013

DOI: 10.1039/c3ta11598d

www.rsc.org/MaterialsA

Published on 05 June 2013. Downloaded by SLUB DRESDEN on 12/07/2013 09:06:08.

1 Introduction

Lithium-metal-oxides with a layer structure have been employed for decades as cathode materials in lithium-ion batteries. Currently, the materials of choice in commercial applications are oxides containing manganese, nickel and cobalt. Considerable research work is currently under way to improve the performance of the battery by modifying the cathode materials. In the present work, we investigate the properties of aluminum-doped $Li_xMn_yNi_zO_2$. Early investigations showed that Al doping increases the structural stability of the monoclinic $LiMnO_2$.[1] Moreover, computational studies suggested a high battery voltage of about 5.4 V for the oxide $LiAlO_2$.[2] However, Al in $LiAlO_2$ is electrochemically inactive. The mixture of Al with electrochemically active transition metal oxides could facilitate the function of the battery at high voltage.[3] Indeed, the computational investigation of $Li(Al_{1/3}Mn_{1/3}Ni_{1/3})O_2$ in ref. 3 predicted an increase in the voltage of more than 0.2 V compared to $Li(Co_{1/3}Mn_{1/3}Ni_{1/3})O_2$. However, $Li(Al_{1/3}Mn_{1/3}Ni_{1/3})O_2$ synthesis invariably led to the formation of a highly defected crystal, very different from the perfect crystal considered in the simulations. Recently, interest in Al doping has been revived.[4–6] Croguennec *et al.* found that aluminum substitution in a nickel manganese cobalt oxide induces a decrease in the reversible capacity, but also a major improvement in the thermal stability.[7] $Li_{1.2}(Al_yCo_{0.08-y}Mn_{0.56}Ni_{0.16})O_2$ was shown to display a high structural stability and a high energy density at low discharge rates.[8] Also Al deposited on $Li(Co_{1/3}Mn_{1/3}Ni_{1/3})O_2$ had positive effects on the electrochemical properties.[9] Still, all these studies focused on compounds with a high content of aluminum and/or a presence of cobalt. However it would be desirable to investigate cobalt-free oxides.

In this work, we consider the possibility that a small concentration of aluminum in a cobalt-free oxide might still have positive effects on the performance of the oxide, while making its synthesis easier. While we cannot predict how to synthesize the compound, *ab initio* simulations have been shown to be effective in predicting several properties directly related to the material's performance. Indeed, to achieve high battery performance, these intercalation compounds should exhibit the following properties: (i) structural stability of the system during Li deintercalation, (ii) easy redox reaction of metal ions (*i.e.* with two stable oxidation states of the metal ions), (iii) high reaction energy of Li intercalation determining the battery voltage, (iv) high Li mobility, and (v) high electronic conductivity. Regarding this last point, we would like to stress that, often, cathode materials are defective band insulators with polaron-mediated electric conductivity. However, polaron conduction is an activated process; therefore, achieving band conductivity might present considerable advantages. In the present work we consider the effect of small amounts of Al doping on cobalt-free oxides. In particular, the oxide $Li(Mn_{0.5}Ni_{0.5})O_2$ is an especially attractive system compared to toxic cobalt-based materials because of its comparatively high capacity ($\sim$200 mA h g^{-1}) and low costs. Its structural and electrochemical properties have been comprehensively investigated both experimentally and theoretically.[10–14]

The ideal rhombohedral layer structure of $Li(Mn_{0.5}Ni_{0.5})O_2$ is shown in Fig. 1a. It has the α-$NaFeO_2$ crystal structure (space

[a]Institute for Materials Science and Max Bergman Center of Biomaterials, TU Dresden, 01062 Dresden, Germany. E-mail: manfred.bobeth@nano.tu-dresden.de
[b]The Abdus Salam International Centre for Theoretical Physics, Strada Costiera 11, 34151 Trieste, Italy
[c]Center for Advancing Electronics Dresden, TU Dresden, 01062, Germany
[d]Division of IT Convergence Engineering, POSTECH, Pohang 790-784, Republic of Korea

Published on 05 June 2013. Downloaded by SLUB DRESDEN on 12/07/2013 09:06:08.

group $R\bar{3}m$). Because of the characteristic zigzag ordering of Ni and Mn atoms in the transition metal (TM) layers (*cf.* Fig. 1b), this configuration is briefly referred to as *zigzag* structure in the following. X-ray and neutron diffraction studies revealed that the arrangement of lithium and transition metals in separate layers is not perfect.[15,16] Small amounts of Ni ions (~10%) have been found in Li layers, as well as Li ions within the TM layers. A theoretical prediction of the phase diagram of $Li(Mn_{0.5}Ni_{0.5})O_2$ in ref. 14 indicated that the zigzag configuration (*cf.* Fig. 1b) of the TM layers (without Li) is the most stable configuration up to 550 °C. At higher temperatures, a partially disordered configuration with a small amount of Li in the TM layers becomes more stable. Li atoms in the TM layers lead to a special atom ordering where Li is surrounded by Mn^{4+} atoms, avoiding Ni^{2+} ions[17] (*cf.* Fig. 1c). This flower-like arrangement is referred to as the *flower* structure in this paper.

The electrochemically inactive Mn^{4+} ions stabilize the structure during Li deintercalation, while Ni^{2+} is oxidized to Ni^{4+} in the fully deintercalated state. For the $Li(Mn_{0.5}Ni_{0.5})O_2$ system, different rechargeable capacities between 140 and 200 mA h g^{-1}, depending on the atom configuration, have been reported.[15,16] This different electrochemical behavior for the same composition has been attributed to the specific ordering of Ni^{2+}, Mn^{4+} and Li^{1+} ions in the system. For Li-rich systems with excess Li in the Ni layers, where Ni atoms in Li layers can be avoided, we expect higher capacity and faster Li migration, compared to stoichiometric $Li(Mn_{0.5}Ni_{0.5})O_2$ with Ni–Li exchange. Recently, the lithium-rich layered compound $Li(Li_{0.2}Ni_{0.2}Mn_{0.6})O_2$ has been synthesized.[18] Interestingly, this system does not separate into the trigonal phases $LiMnO_2$ and Li_2MnO_3, but forms a solid solution. The crystal structure of $Li(Li_{0.2}Ni_{0.2}Mn_{0.6})O_2$ is monoclinic (space group $C2/m$). This system is especially interesting since it exhibits a comparatively high capacity because of the higher lithium content. For a similar Li-rich system with $Li(Li_{1/6}Ni_{1/6}Mn_{2/3})O_2$ stoichiometry, the monoclinic structure and the corresponding atomic arrangement in the TM layers are shown in Fig. 1d and e, respectively. This particular ordered structure was suggested by Jarvis *et al.*[18] In the following, calculations will be performed also for this system, which will be denoted as the *Li-rich* structure for brevity.

While there are many studies on the electrochemical properties of the Li–Ni–Mn–O system, only a few studies concern the effects of dopants in this system. In particular, only Al-containing oxides with a high Al content have been considered so far. In this work, we investigate the effects of Al-doping on the structure and properties of the Li–Mn–Ni–O system. To this end, we consider the rhombohedral layer structure of $Li(Mn_{0.5}Ni_{0.5})O_2$ as well as the Li-rich monoclinic layer structure of $Li(Li_{1/6}Mn_{2/3}Ni_{1/6})O_2$ as base structures. We introduce a level of doping smaller than those considered in previous studies, leading to the stoichiometries $LiAl_{1/12}Mn_{1/2}Ni_{5/12}O_2$ for the rhombohedral layer structure and $Li(Li_{1/6}Al_{1/6}Mn_{1/2}Ni_{1/6})O_2$ for the Li-rich monoclinic structure. Thus aluminum occupies 1/6 and 1/3 of the nickel sites in the two cases. Though this might seem a high doping concentration, in fact most previous studies considered even higher doping concentrations. For example, in ref. 3 the stoichiometry $Li(Al_{1/3}Mn_{1/3}Ni_{1/3})O_2$ was considered. The smaller doping considered in the present work might be of help to overcome problems observed in previous work, such as high concentration of defects, reducing structural stability (ref. 3), and a decrease in reversible capacity (ref. 7). From the point of view of electronic structures, these stoichiometries are especially interesting because they represent two very different cases. In $LiAl_{1/12}Mn_{1/2}Ni_{5/12}O_2$, nickel (formally Ni^{2+}) is substituted by Al^{3+}, thereby creating uncompensated charges. In contrast, in $Li(Li_{1/6}Al_{1/6}Mn_{1/2}Ni_{1/6})O_2$, Ni^{2+} is substituted in equal proportions by Li^+ and Al^{3+} such that charge compensation is maintained. We will show that this has dramatic consequences on the electronic structure, with the charge-compensated oxide being a band insulator, and the uncompensated oxide being a band conductor. *Ab initio* total energy calculations were performed to determine the electrochemical properties of the undoped and Al-doped systems at zero temperature.

The paper is outlined as follows. After a brief presentation of the theoretical method, we report on the calculated atomic and electronic structures of the systems. Thereafter, important properties for a successful cathode material such as the structural stability during Li deintercalation, the electrochemical behavior, the battery voltage, and the Li mobility are considered.

2 Computational details

Computations of the atomic and electronic structures of the mixed metal oxides were carried out within the framework of spin polarized density-functional theory (DFT), using the Vienna *ab initio* simulation package (VASP).[19–21] For the exchange–correlation functional the PBE generalized gradient approximation (GGA)[22] was used, and the PAW method[23,24] was applied to describe the interaction between valence electrons and core ions. Due to strongly correlated d bands in the transition metals Mn and Ni, the GGA+U approach with $U = 5.0$ eV for Mn and $U = 5.9$ eV for Ni, as suggested by previous DFT calculations,[14] was applied in all calculations. The wave functions were expanded in plane waves up to a kinetic energy cutoff of 520 eV. For the three considered oxide structures shown in Fig. 1, different simulation cells were used: (i) a 2×2 unit cell for the rhombohedral structure with zigzag configuration (total 48 atoms), (ii) a $2\sqrt{3} \times 2\sqrt{3}$ unit cell for the rhombohedral structure with flower configuration (total 144 atoms), and (iii) a 1×6 unit cell for the Li-rich monoclinic structure (total 24 atoms). In the case of the rhombohedral crystal structure, integration in the first Brillouin zone was performed using Monkhorst–Pack grids including 32 and 9 k-points in the primitive cell for the zigzag and flower configurations, respectively. For the monoclinic structure, 36 k-points were used. For all considered crystal structures, the atomic coordinates, as well as the shape and volume of the unit cell, were optimized until the force components were less than 10^{-3} eV $Å^{-1}$.

In this work we have considered only the total energies of the different configurations, neglecting entropic contributions to the free energy. Entropic contributions come from vibrational,

 This journal is © The Royal Society of Chemistry 2013

Published on 05 June 2013. Downloaded by SLUB DRESDEN on 12/07/2013 09:06:08.

configurational and electronic degrees of freedom. It is known that, for heavier elements, vibrational degrees of freedom give a contribution of a few tens of meV at most at room temperature, including zero-point energies.[25,26] In the case of lithium, it has been shown that these contributions are smaller than 0.1 eV per Li atom in lithium oxides[27] and smaller than 30 meV in lithium manganese oxides at room temperature,[28] *i.e.* they can be safely neglected in solids in a first approximation. In non-stoichiometric cases, the configurational entropy sometimes gives a larger contribution than the vibrational entropy.[29] Although in some cases configurational and electronic degrees of freedom can be fundamental in determining the equilibrium between ordered and disordered phases, their contribution is rather small at room temperature. Zhou *et al.* explicitly calculated the entropic contributions from electronic and configurational degrees of freedom for Li_2FePO_4, and found them to be important for phase separation in that system.[30] Still, also in that case the total entropy was less than 1 k_B, *i.e.* contributing less than 25 meV per Li atom to the free energy at room temperature.[30] This is true also for different solid state systems such as defective CeO_2.[31] Experimentally, Stevens *et al.* measured vibrational and configurational entropy differences of $\sim$3 J K^{-1} mol^{-1} at most for lithium iron phosphate phases.[32] This corresponds to contributions to the free energy of roughly 10 meV at room temperature. In the following, we have taken care that our conclusions are robust against uncertainties in the free energies of the order of tens of meV per Li atom. In this way, we can ensure that neglecting these entropic contributions does not affect our conclusions. We would like to stress that this would not be possible if we were interested in a detailed description of lithium and defect ordering in the material. Finally, we must consider the possibility that, although entropic contributions are small, our choice of configurations is restricted and, for this reason, we might miss some relevant configurations. First, this problem is relevant for defective systems and not for the stoichiometric compounds. If we missed some low-energy configurations, this would strengthen our conclusion that the mixed, defective, non-stoichiometric system is stable against phase separation into the stoichiometric end-phases. Moreover, regarding lithium migration, we have considered only the diluted limit where the migrating lithium is essentially isolated from the others, and therefore the precise order of lithium ions and vacancies is not relevant.

3 Atomic and electronic structures

To determine the atomic structure and electronic properties of the oxide structures in Fig. 1 we calculated the total energies and the density of states (DOS) of these systems. The calculated total energies per formula unit for the zigzag and flower structures of $Li(Mn_{0.5}Ni_{0.5})O_2$ showed that the zigzag structure is energetically more favorable by 45 meV at zero temperature. This result is in agreement with theoretical investigations reported in ref. 14, where the zigzag structure of the TM layers (without Li) was predicted as the most stable configuration up to 550 °C, followed by a partially disordered flower configuration (with a small amount of Li in the TM layers) at higher temperatures. To analyze the effect of Al-doping on the electrochemical behavior, we randomly replaced Ni atoms of the oxide structures by Al, corresponding to the compound $LiAl_{1/12}Mn_{1/2}Ni_{5/12}O_2$. For both zigzag and flower structures, Ni atoms in the TM layers were replaced by Al. For the flower structure, additionally the case of replacement of only Ni in the Li layers was considered. The difference in the total energies of those two flower configurations is about 50 meV, revealing a favored location of Al in the TM layers. The Li-rich monoclinic structure with atom ordering in the TM layers as shown in Fig. 1e has only one Ni atom in the TM layer of the simulation cell. Thus, for this structure, one Mn atom is replaced by an Al atom, corresponding to the composition $Li(Li_{1/6}Al_{1/6}Mn_{1/2}Ni_{1/6})O_2$.

Calculations of the electronic structure of $Li(Mn_{0.5}Ni_{0.5})O_2$ in the literature[11] revealed that the total energy of the system essentially depends on the spin ordering. For the zigzag structure, we found that the Ni spins are antiferromagnetically aligned with the Mn spins in the TM layers. The ferromagnetic spin ordering of the TM atoms is energetically less favorable by 0.1 eV per unit cell. For the flower structure, we found in agreement with the GGA+*U* calculations in ref. 11 that the Ni spins in the Li layers are aligned antiferromagnetically with the Ni atoms in the TM layers. The Mn spins exhibit an antiferromagnetic layer-by-layer arrangement. Ni and Mn atoms within a TM layer show a complex ferro- and antiferromagnetic ordering. In the case of the Li-rich system, the antiferromagnetic arrangement of Ni and Mn atoms in the TM layer is energetically more stable by 0.22 eV than the ferromagnetic ordering. Because of the small size of the monoclinic unit cell used in the calculations (only one TM layer in the unit cell), the antiferromagnetic layer-by-layer arrangement was excluded. The calculated structure parameters and spin polarization data for the considered undoped and Al-doped crystal structures are listed in Table 1. Thereby, $E_{FM} - E_{AFM}$ is the difference in the total energies of the ferromagnetic and antiferromagnetic spin arrangements, and μ_B is the magnetic moment of the transition metal atoms in the TM layers for the most favorable spin ordering. For all considered systems, the antiferromagnetic spin ordering within the TM layers is preferred. The Al-doped systems show a smaller energy difference between the two spin states because the Al atoms are not spin-polarized.

To further characterize the electronic structure of the Al-doped oxides, the calculated total and partial densities of states are shown in Fig. 2. For all oxide systems, the empty spin-down and spin-up e_g states indicate an electronic configuration of t_{2g}^3 for Mn ions corresponding to Mn^{4+}. The densities of states of the Ni ions show that the e_g up state is unoccupied corresponding to the state $t_{2g}^6e_g^2$ or to Ni^{2+}. Looking at the total densities of states, no band gap is observed for the zigzag and flower structures, while a band gap of 0.89 eV is found for the Li-rich structure. This is consistent with an analysis of the formal oxidation states of these compounds. Indeed, for the Li-rich monoclinic compound with $Li(Li_{1/6}Al_{1/6}Mn_{1/2}Ni_{1/6})O_2$ stoichiometry the charges are well compensated: for each divalent Ni ion substituted by a monovalent Li ion there is another divalent Ni ion substituted by a trivalent Al ion. This explains why this compound is found to be a band insulator in our calculations.

Published on 05 June 2013. Downloaded by SLUB DRESDEN on 12/07/2013 09:06:08.

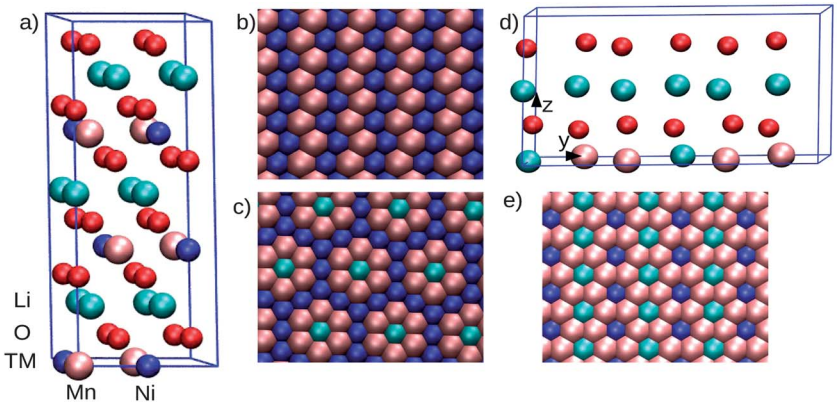

Fig. 1 Illustration of the considered undoped crystal structures: rhombohedral layer structure of Li($Mn_{1/2}Ni_{1/2}$)O_2 (a), the zigzag (b) and flower (c) configurations of mixed Mn–Ni layers, the Li-rich monoclinic lattice structure of Li($Li_{1/6}Mn_{2/3}Ni_{1/6}$)O_2 (d), and the corresponding atomic configuration of the mixed TM layer (e). The transition metals, Ni and Mn, as well as oxygen and lithium are labeled in (a). For the flower configuration, 16.7% of the Ni atoms in the TM layers are exchanged with Li atoms in the Li layers.

Table 1 Lattice parameters and electronic structure properties of Li–Mn–Ni–O and Al doped Li–Mn–Ni–O systems. In the first column, the composition is given. The second column (Str.) denotes the considered rhombohedral zigzag (Z) and flower (F) configurations, and the Li-rich (R) monoclinic structures. Columns *a*, *b* and *c* represent the lattice constants in Angstroms. $E_{FM} - E_{AFM}$ (in eV) is the difference in the total energies of the ferromagnetic (FM) and antiferromagnetic (AFM) spin ordering. μ_B (in Bohr magnetons) is the magnetic moment of the spin-polarized elements

Compound	Str.	*a*	*b*	*c*	$E_{FM} - E_{AFM}$	μ_B (Mn)	μ_B (Ni)
$LiMn_{1/2}Ni_{1/2}O_2$	Z	2.94	2.94	14.44	0.10	3.40	1.76
$LiMn_{1/2}Ni_{1/2}O_2$	F	2.92	2.92	14.41	0.26	3.31	1.74
$Li[Li_{1/6}Mn_{2/3}Ni_{1/6}]O_2$	R	4.98	8.62	5.08	0.22	3.60	1.76
$LiAl_{1/12}Mn_{1/2}Ni_{5/12}O_2$	Z	2.91	2.91	14.45	0.08	3.46	1.76
$LiAl_{1/12}Mn_{1/2}Ni_{5/12}O_2$	F	2.90	2.90	14.41	0.09	3.45	1.76
$Li[Li_{1/6}Al_{1/6}Mn_{1/2}Ni_{1/6}]O_2$	R	4.97	8.62	5.08	0.02	3.37	1.76

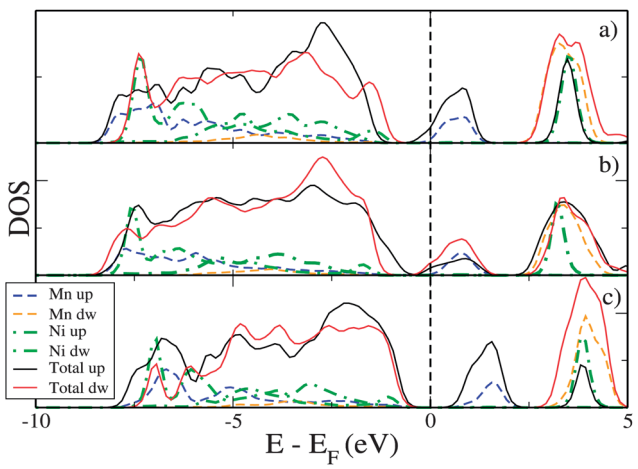

Fig. 2 Total and partial densities of states (DOS) for the transition metals Mn and Ni with different spin polarizations, up and down (dw), in the Li–Al–Mn–Ni–O system with zigzag (a), flower (b), and Li-rich (c) crystal structures.

On the other hand, the $LiAl_{1/12}Mn_{1/2}Ni_{5/12}O_2$ stoichiometry of the rhombohedral compounds produces an excess of one hole per Al atom. The consequence, well reproduced by the calculated DOS, is that no gap is observed for the rhombohedral structures. A question may arise as to where the additional charge goes in the uncompensated case. From the DOS (Fig. 2) we can see that the band, which becomes partially filled, has mainly Mn character. Typically, it is expected that the charge will form a Mn^{3+} with polaronic distortion, but this effect is usually missed in standard DFT.[33–35] A study of the polaronic distortion is possible by employing hybrid functionals, but this goes beyond the scope of the present paper and will be a subject of future research. This analysis of the role of the Mn ions is confirmed by an analysis of the magnetic moments reported in Table 1. Introducing Al in the zigzag and flower structures leads to uncompensated charges and therefore to slightly reduced Mn ions. This is reflected by a slight increase of the magnetic moment of the Mn ions in these cases. In contrast, Al doping of the Li-rich structure creates a situation of perfect charge compensation, and as a consequence the magnetic moment of the Mn ions increases.

The effect of Al doping on the electric conductivity is very different in the three compounds. We reach this conclusion by analyzing the electronic density of states (DOS), and changes in the DOS induced by Al doping (Fig. 2). The conductive behavior crucially depends on the stoichiometry of the compound. In fact, from our study we find that the only factor influencing the band conductivity is the charge compensation of the compound. Since Al^{3+} substitutes Ni^{2+} ions, this introduces uncompensated charges in systems that were charge

 This journal is © The Royal Society of Chemistry 2013

Published on 05 June 2013. Downloaded by SLUB DRESDEN on 12/07/2013 09:06:08.

compensated. As can be seen from the calculated DOS, this results in a metallic character of the electronic structure. This happens for the zigzag and flower structures. On the other hand, the effect of Al doping on the Li-rich structure is to compensate the Li doping, thereby compensating previously uncompensated charges. As the final result, this compound becomes a band insulator upon doping, as shown in Fig. 2c. Still it is probable that, in the presence of an insulating band structure, the main conductivity mechanism is the hopping of polarons, as is often the case in cathode materials. A description of polarons by density functional theory (DFT) and post-DFT methods is non-trivial and goes beyond the scope of the present paper.

4 Structural stability

A very important precondition for the application of metal oxides as cathode materials is their structural stability during lithium deintercalation. For instance, complete removal of lithium from $LiCoO_2$ causes oxygen rearrangement in CoO_2 into hexagonal close packing. Only 50% of Li can be reversibly removed without essential changes of the host structure, limiting the charge capacity of $LiCoO_2$. Several additions have been suggested to improve the structural stability of host materials and, consequently, the cycling capacity of batteries. For example, in the case of the spinel structure of $LiMn_2O_4$, stabilization is achieved by simultaneous doping with Al and F, leading to $Li_{1+x}Mn_{1-x-y}Al_yO_{4-z}F_z$.[36] The structural stability of layered lithium oxides is strongly related to the behavior of Li vacancies in the Li layers. To stabilize the system, the vacancies should be distributed as uniformly as possible. From a theoretical point of view, the stability can be characterized by calculating the formation energy of different Li vacancy arrangements as a function of the Li concentration x ($0 < x < 1$) in the layers.[37] The Li-vacancy ordering in the Li layers crucially determines the value of the formation energy. Calculations at fixed concentration x were performed for several vacancy arrangements. The formation energies reported here correspond to the energetically most favorable Li-vacancy ordering which we found.

The formation energy of a partially lithiated system is defined as

$$E_F = E(Li_xMO_2) - xE(LiMO_2) - (1 - x)E(MO_2) \quad (1)$$

where $E(Li_xMO_2)$ is the total energy of the energetically most favorable vacancy configuration, and $E(LiMO_2)$ and $E(MO_2)$ are the energies of the completely intercalated and deintercalated systems, respectively. Negative values of the formation energy indicate that the system is stable with respect to phase separation into $LiMO_2$ and MO_2. Phase separation causes a structure instability if the fully delithiated system is unstable. Concerning the Li–Mn–Ni–O system, we calculated the corresponding formation energies for the undoped system $Li_xMn_yNi_{1-y}O_2$ and the Al-doped system $Li_xAl_zMn_yNi_{1-y-z}O_2$. The calculated formation energies are shown in Fig. 3 as a function of the Li concentration. All the structures considered have negative

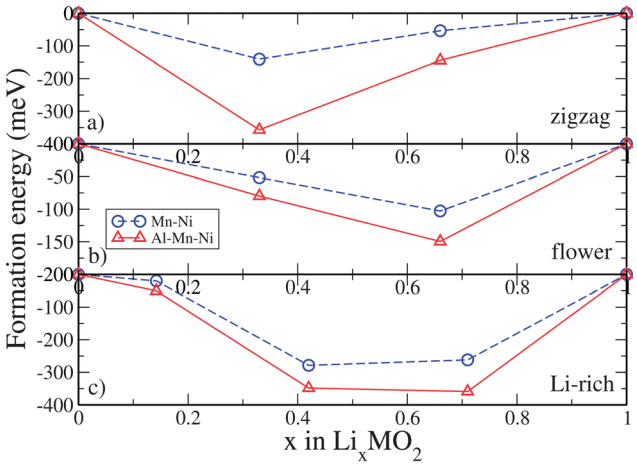

Fig. 3 Formation energies of Li_xMO_2 as a function of the Li concentration for doped (triangles) and undoped (circles) Li–Mn–Ni–O structures: zigzag, flower, and Li-rich. Lines are drawn to guide the eye.

formation energies, *i.e.* phase separation into $LiMO_2$ and MO_2 should not occur. The formation energies of the Al-doped systems are more negative than those of the undoped ones. Thus, Al-doping stabilizes the layered structures at all Li concentrations, and helps avoiding irreversible phase transformations in the cathode material.

5 Electrochemical behavior

To evaluate the electrochemical activity of the Li–Al–Mn–Ni–O system, we calculated the change of the partial charges of the metal ions during Li intercalation by means of the Bader charge analysis[38] as implemented in VASP.[39] The partial charges of the metal ions in the Al-doped systems are shown in Fig. 4 as a function of the Li concentration for the zigzag and Li-rich structures. For these structures, remarkable changes of partial charges are observed only for the Ni ions. The partial charges of

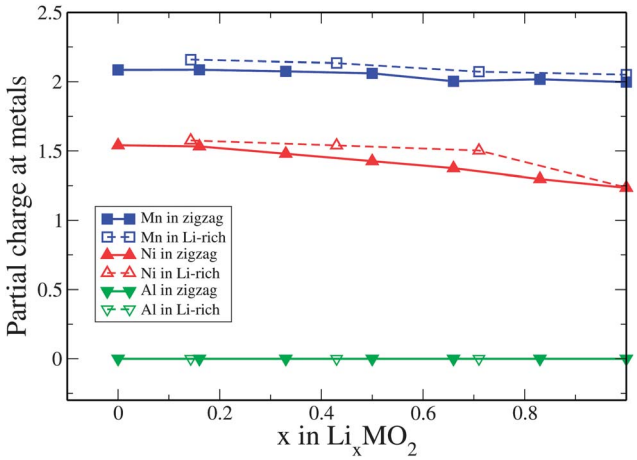

Fig. 4 Net populations of the valence orbitals of the metals Al, Mn, and Ni from the Bader analysis as a function of the Li concentration for the zigzag and Li-rich structures of the Li–Al–Mn–Ni–O system.

Published on 05 June 2013. Downloaded by SLUB DRESDEN on 12/07/2013 09:06:08.

Mn and Al ions remain almost constant during Li intercalation. Also, the different atomic structure of the oxides does not essentially affect the value of the partial charges of the metal ions. For the flower configuration (not shown), almost the same charge values were obtained as for the zigzag configuration. Since Al is electrochemically inactive and substitutes the electrochemically active nickel, Al-doping reduces the overall electrochemical activity of the cathode material.

6 Battery voltage

In this section, we present our calculated voltage–composition curve of the battery. The voltage between the two electrodes can be expressed by the difference of the chemical potential of Li between the anode and cathode. Bulk Li metal is chosen as the anode. Then, the average voltage V at zero temperature can be derived from total energy calculations *via* the formula[2,37]

$$V = \frac{E(\mathrm{Li}_{x_1}\mathrm{MO}_2) - E(\mathrm{Li}_{x_2}\mathrm{MO}_2) + (x_2 - x_1)\,E^{\mathrm{bulk}}(\mathrm{Li})}{(x_2 - x_1)\,e} \quad (2)$$

where $E(\mathrm{Li}_{x1}\mathrm{MO}_2)$ and $E(\mathrm{Li}_{x2}\mathrm{MO}_2)$ are the total energies of the systems with the Li concentrations x_1 and x_2. $E^{\mathrm{bulk}}(\mathrm{Li})$ is the total energy of Li metal in a bcc structure, corresponding to the chemical potential of Li in the anode. In the case of the flower and Li-rich structures, where a part of Li is also arranged in the TM layers, we removed Li only from the Li layers. The total energies used for the voltage calculations were always the values of those Li-vacancy arrangements where we found the lowest total energy. The calculated average voltages are shown in Fig. 5 as a function of the Li concentration for the undoped and Al-doped structures. As a result, we find that for the zigzag configuration, the Al-doped system leads to higher voltages at all Li concentrations. At Li concentrations near $x \sim 0.5$, where the host structure is still stable, the voltage is 4.01 V for the undoped system and 4.24 V for the Al-doped system. Remarkably, a particularly high voltage, compared to the other structures, is observed for the Li-rich structure. For this structure, the average voltage increases due to doping from 5.31 V to 5.60 V near 60% Li concentration.

Though in some cases the voltage of the undoped material is slightly higher, overall the energy densities increase under all circumstances because of the much lower weight of aluminum with respect to nickel. To assess the overall effect, we have calculated energy densities with respect to the weight of the fully lithiated oxide using the data shown in Fig. 5. It should be noted that this overestimates the energy density, because it neglects the presence of other components of the battery, such as electrolyte, separators and contacts. For the zigzag structure, the energy density increases from 1096 W h kg^{-1} to 1213 W h kg^{-1} upon Al doping; for the flower structure it increases from 1030 to 1072 W h kg^{-1}, and for the Li-rich structure from 1352 to 1565 W h kg^{-1}.

7 Li diffusion barrier

An important feature to achieve high battery power is a fast migration of Li ions into the host material. The Li intercalation and deintercalation are complex processes which strongly depend on the Li concentration in the Li layers owing to the interaction between the Li ions. Depending on the arrangement of Li vacancies in the Li layers, the Li ions have different local environments, determining the activation energies for jumps of Li ions from site to site in the Li layers. For a first evaluation of the Al-doping effect, we consider here the migration of Li ions in the dilute limit, where the Li layers are almost empty. The activation energy for Li migration was determined by *ab initio* calculations, using the nudged elastic band method.[40] According to this method, the maximum energy along the minimum energy path between two neighboring Li sites is obtained.

In the case of the flower structure, a configuration was considered where a Li atom is as far as possible from the Ni atoms in the Li layer. Thus, a strong Li–Ni interaction is avoided so that a comparatively small activation energy results. In Fig. 6, the calculated energy profiles of Li migration from one octahedral site to the neighboring octahedral site are shown for

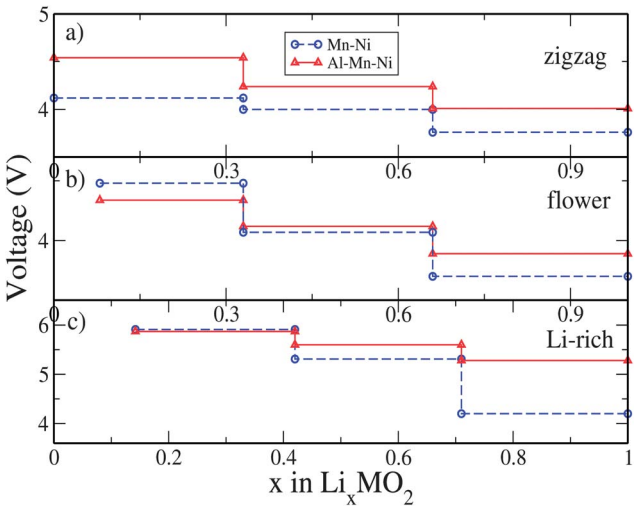

Fig. 5 Calculated average voltages for undoped (circles) and Al-doped (triangles) metal oxides with zigzag, flower, and Li-rich structures.

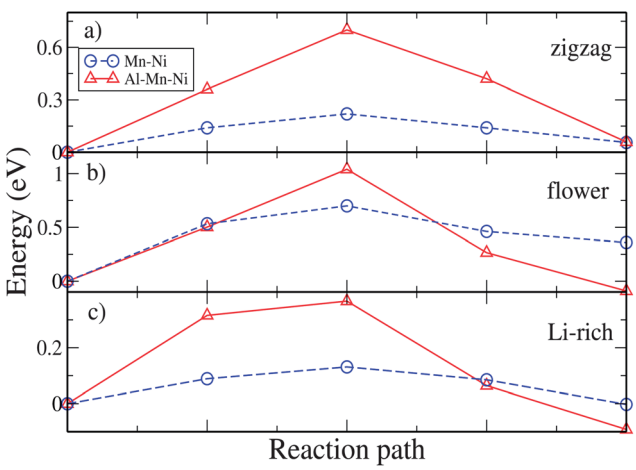

Fig. 6 Calculated energy profiles of Li migration from one octahedral site to a neighboring octahedral site (from left to right) in different undoped (Li–Mn–Ni–O, circles) and Al-doped (Li–Al–Mn–Ni–O, triangles) oxide systems.

This journal is © The Royal Society of Chemistry 2013

Published on 05 June 2013. Downloaded by SLUB DRESDEN on 12/07/2013 09:06:08.

different oxide structures. The asymmetric form of energy profiles is caused by the corresponding nonequivalent initial and final Li positions in the multi-component host material. The profiles indicate that Al-doping increases the activation barrier for all considered structures and, consequently, decreases the Li mobility. The activation barrier increases by 0.2–0.5 eV, depending on the structure. This should result in a measurable increase of the overpotentials, and a corresponding decrease of the efficiency of the battery. The highest activation energy of about 1 eV was found for the Al-doped flower configuration. The undoped Li-rich structure shows the smallest activation energy of only 0.15 eV.

8 Conclusions

The effect of Al-doping of rhombohedral and monoclinic layered structures of $Li_xMn_yNi_{1-y}O_2$ on their suitability as cathode materials was investigated within the framework of density-functional theory. The calculated formation energies of Li-vacancy arrangements in the Li layers suggest a stabilizing effect of Al-doping for all structures considered. The derived battery voltages at zero temperature are enhanced by Al-doping, except for the Li-rich monoclinic oxide at low Li concentration. Comparatively high voltages were obtained for the doped Li-rich monoclinic structure. In this case, Al-doping remarkably diminishes the voltage decay with increasing Li intercalation. Moreover, as a consequence of voltage changes and the low weight of aluminum, the energy density of the battery is increased in all cases. In contrast to these positive effects, the Li mobility at low Li concentration is obviously reduced by Al-doping as suggested by the calculated activation energies for Li jumps. Among the doped systems, the Li-rich monoclinic structure exhibits the smallest activation energy. In summary, the Al-doped Li-rich monoclinic structure seems to be most promising as a cathode material because of a comparatively high battery voltage.

Acknowledgements

The authors thank Dr Mihails Kusnezoff and Dr Michael Schneider for fruitful discussions. Computational resources were provided by the Center for Information Services and High Performance Computing (ZIH) of the Technische Universität Dresden. This work was funded by the European Union (ERDF) and the Free State of Saxony *via* TP A2 ("MolFunc"/"MolDiagnosik") of the Cluster of Excellence "European Center for Emerging Materials and Processes Dresden" (ECEMP) and by the World Class University program funded by the Ministry of Education, Science and Technology through the National Research Foundation of Korea (R31-10100). We gratefully acknowledge support from the German Excellence Initiative *via* the Cluster of Excellence EXC 1056 "Center for Advancing Electronics Dresden" (cfAED).

References

1 Y. Jang, W. D. Moorehead and Y. M. Chiang, *Solid State Ionics*, 2002, **149**, 201.
2 M. K. Aydinol, A. F. Kohan and G. Ceder, *Phys. Rev. B: Condens. Matter Mater. Phys.*, 1997, **56**, 1354.
3 S. K. Hu, T. C. Chou, B. J. Hwang and G. Ceder, *J. Power Sources*, 2006, **160**, 1287.
4 S.-M. Dou, W.-L. Wang, H.-J. Li and X.-D. Xin, *J. Solid State Electrochem.*, 2011, **15**, 747.
5 Y.-K. Lin and C.-H. Lu, *J. Power Sources*, 2009, **189**, 353.
6 G.-B. Zhong, Y.-Y. Wang, X.-J. Zhao, Q. S. Wang, Y. Yu and C.-H. Chen, *J. Power Sources*, 2012, **216**, 368.
7 L. Croguennec, J. Bains, J. Breger, C. Tessier, P. Biensan, S. Levasseur and C. Delmas, *J. Electrochem. Soc.*, 2011, **158**, A664.
8 Z. Li, N. A. Chernova, J. Feng, S. Upreti, F. Omenya and M. S. Whittingham, *J. Electrochem. Soc.*, 2012, **159**, A116.
9 T. E. Hong, E. D. Jeong, S. R. Baek, M. R. Byeon, Y. S. Lee, F. N. Khan and H. S. Yang, *J. Appl. Electrochem.*, 2012, **42**, 41.
10 Y. S. Meng, G. Ceder, C. P. Grey, W. S. Yoon and Y. Shao-Horn, *Electrochem. Solid-State Lett.*, 2004, **7**, A155.
11 A. Van der Ven and G. Ceder, *Electrochem. Commun.*, 2004, **6**, 1045.
12 J. Breger, Y. S. Meng, Y. Hinuma, S. Kumar, K. Kang, Y. Shao-Horn, G. Ceder and C. P. Grey, *Chem. Mater.*, 2006, **18**, 4768.
13 J. Breger, K. Kang, J. Cabana, G. Ceder and C. P. Grey, *J. Mater. Chem.*, 2007, **17**, 3167.
14 Y. Hinuma, Y. S. Meng, K. Kang and G. Ceder, *Chem. Mater.*, 2007, **19**, 1790.
15 Y. Makimura and T. Ohzuku, *J. Power Sources*, 2003, **119**, 156.
16 Z. Lu, L. Y. Beaulieu, R. A. Donaberger, C. L. Thomas and J. R. Dahn, *J. Electrochem. Soc.*, 2002, **149**, A778.
17 W. S. Yoon, S. Iannopollo, C. P. Grey, D. Carlier, J. Gorman, J. Reed and G. Ceder, *Electrochem. Solid-State Lett.*, 2004, **7**, A167.
18 K. A. Jarvis, Z. Deng, L. F. Allard, A. Manthiram and P. J. Ferreira, *Chem. Mater.*, 2011, **23**, 3614.
19 G. Kresse and J. Furthmueller, *Phys. Rev. B: Condens. Matter Mater. Phys.*, 1996, **54**, 11169.
20 G. Kresse and J. Hafner, *Phys. Rev. B: Condens. Matter Mater. Phys.*, 1994, **558**, 14251.
21 G. Kresse and D. Joubert, *Phys. Rev. B: Condens. Matter Mater. Phys.*, 1999, **59**, 1758.
22 J. P. Perdew, K. Burke and M. Ernzerhof, *Phys. Rev. Lett.*, 1996, **77**, 3865.
23 P. Bloechl, *Phys. Rev. B: Condens. Matter Mater. Phys.*, 1994, **50**, 17953.
24 G. Kresse and J. Furthmueller, *J. Comp. Mater. Sci.*, 1996, **6**, 15.
25 K. Reuter and M. Scheffler, *Phys. Rev. B: Condens. Matter Mater. Phys.*, 2001, **65**, 035406.
26 N. Seriani, W. Pompe and L. Colombi Ciacchi, *J. Phys. Chem. B*, 2006, **110**, 14860.
27 N. Seriani, *Nanotechnology*, 2009, **20**, 445703.
28 S. K. Mishra and G. Ceder, *Phys. Rev. B: Condens. Matter Mater. Phys.*, 1999, **59**, 6120.
29 M. E. Arroyo y de Dompablo, A. Van der Ven and G. Ceder, *Phys. Rev. B: Condens. Matter Mater. Phys.*, 2002, **66**, 064112.
30 F. Zhou, T. Maxisch and G. Ceder, *Phys. Rev. Lett.*, 2006, **97**, 155704.

31 C. B. Gopal and A. van de Walle, *Phys. Rev. B: Condens. Matter Mater. Phys.*, 2012, **86**, 134117.
32 R. Stevens, J. L. Dodd, M. G. Kresch, R. Yazami, B. Fultz, B. Ellis and L. F. Nazar, *J. Phys. Chem. B*, 2006, **110**, 22732.
33 S. Sicolo, G. Palma, C. Di Valentin and G. Pacchioni, *Phys. Rev. B: Condens. Matter Mater. Phys.*, 2007, **76**, 075121.
34 S. P. Ong, Y.-F. Mo and G. Ceder, *Phys. Rev. B: Condens. Matter Mater. Phys.*, 2012, **85**, 081105.
35 J. B. Varley, A. Janotti, C. Franchini and C. G. Van de Walle, *Phys. Rev. B: Condens. Matter Mater. Phys.*, 2012, **85**, 081109.
36 G. G. Amatucci, N. Pereira, T. Zheng and J. M. Tarascon, *J. Electrochem. Soc.*, 2001, **148**, A171.
37 Y. S. Meng and M. E. Arroyo de Dompablo, *Energy Environ. Sci.*, 2009, **2**, 589.
38 R. F. W. Bader, *Atoms in Molecules: A Quantum Theory*, Oxford University Press, 1994.
39 G. Henkelman, A. Arnaldsson and H. Jonsson, *Comput. Mater. Sci.*, 2006, **36**, 354.
40 H. Jonsson, G. Mills and K. W. Jacobson, *Nudged Elastic Band Method for Finding Minimum Energy Paths of Transitions*, ed. B. J. Byrne, G. Ciccotti and D. F. Coker, World Scientific Publishing Company, River Edge, NJ, 1998.

Published on 05 June 2013. Downloaded by SLUB DRESDEN on 12/07/2013 09:06:08.

This journal is © The Royal Society of Chemistry 2013